Use of a Finite-Element Method to Interpret Rheological Effects in Blade Coating

Data and finite-element simulations are presented for the blade coating of a series of Newtonian and non-Newtonian fluids. Numerical simulations for purely viscous fluids show good agreement with coating thickness data for Newtonian and relatively inelastic non-Newtonian liquids, including geometries for which lubrication theory is inaccurate. These simulations account for the shape of the free surface, with surface tension included, and incorporate realistic inflow and outflow boundary conditions. By comparing pressure distributions generated with the finite-element technique to those calculated using lubrication theory, it is shown that the simple lubrication theory analysis suffers from inadequate inflow and outflow boundary conditions. Comparison of these simulations with new experimental results for three well-characterized viscoelastic liquids, having nearly identical steady shear viscosities but different normal stress behavior, confirms speculations of earlier work with respect to the effect fluid rheology has on coating thickness.

Tim Sullivan, Stanley Middleman
Department of AMES/Chemical Engineering and
Center for Magnetic Recording Research
University of California, San Diego
La Jolla, CA 92093

Roland Keunings
Center for Advanced Materials
Lawrence Berkeley Laboratory
University of California, Berkeley
Berkeley, CA 94720

Introduction

A number of commercial methods used to distribute thin films of liquid onto rapidly moving substrates share several common features with respect to their fluid dynamics. Chief among these features is that they are essentially *lubrication flows* characterized by nearly parallel flow between solid surfaces whose separation is small in comparison to their extent in the primary direction of flow. A typical coater geometry, the blade-over-roll coater, is illustrated in Figure 1. Such a coater is often used to produce thin layers of adhesives, protective polymeric films, photographic emulsions, and magnetic dispersions, and the corresponding liquids are typically non-Newtonian. While coating flows are relatively simple, they are not steady viscometric (simple shear) flows (Middleman, 1977). As a consequence, it is not obvious *a priori* that the viscometric behavior of these fluids is sufficient to define the coating dynamics.

The goal of this and earlier work (Sullivan and Middleman, 1986) has been to examine the coating behavior of a series of non-Newtonian liquids, selected in such a way that it might be possible to separate the effects of several aspects of non-Newtonian rheology on coating performance. In particular, we wish to know how two major characteristics of non-Newtonian liquids, namely the nonlinear shear viscosity, and elasticity as measured by the steady primary normal stress difference, affect the coating thickness achieved with a blade coater.

In our previous study (Sullivan and Middleman, 1986), classical lubrication theory (Cameron, 1966) was extended to permit predictions of coating thickness for purely viscous non-Newtonian liquids. Deviations of the data from theory were observed, but it could not be concluded that these deviations were entirely rheological phenomena, because the lubrication theory model utilized simplified boundary conditions at the inlet and outlet regions of the blade (i.e., ambient pressure) and did not account for inertial effects associated with the flow.

The present work is distinguished from our earlier study, in that the finite-element method (Zienkiewicz, 1977) has been used to produce a solution to the full two-dimensional equations of flow with realistic inflow and outflow boundary conditions. The free-boundary region downstream of the blade is part of the calculation scheme in order to account for exit effects, including those associated with surface tension. Similarly, the computational domain is extended upstream of the blade to minimize any restriction on flow development in the entrance region. The equations of flow are solved with a purely viscous non-Newtonian constitutive equation (four-parameter Carreau model) used to represent the stress terms. Consequently, deviations of the data from the predictions of the finite-element method (FEM) may be interpreted as rheological phenomena other than those associated with nonlinear viscous effects.

The present address of Tim Sullivan is AT&T Bell Laboratories, Murray Hill, NJ 07974.

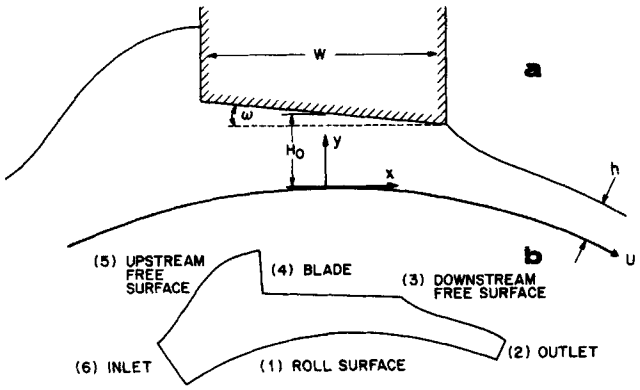

Figure 1. (a) Geometry and coordinates of blade-over-roll coating system; (b) diagram for discussing boundary conditions.

Dynamic Equations and Boundary Conditions

Figure 1a defines the geometry and coordinate system for the blade-over-roll coater of interest. For an assumed two-dimensional, isothermal, steady flow field, the velocity, pressure, and stress components satisfy the following equation set:

$$\rho\left(u\frac{\partial u}{\partial x}+v\frac{\partial u}{\partial y}\right)=-\frac{\partial p}{\partial x}+\frac{\partial \tau_{xx}}{\partial x}+\frac{\partial \tau_{xy}}{\partial y} \tag{1}$$

$$\rho\left(u\frac{\partial v}{\partial x}+v\frac{\partial v}{\partial y}\right)=-\frac{\partial p}{\partial y}+\frac{\partial \tau_{xy}}{\partial x}+\frac{\partial \tau_{yy}}{\partial y} \tag{2}$$

$$\frac{\partial u}{\partial x}+\frac{\partial v}{\partial y}=0 \tag{3}$$

It is assumed here that no significant body forces act in the coating process of interest.

We use a purely viscous constitutive equation in the form

$$\tau=\eta(\Delta)\Delta \tag{4}$$

and choose a four-parameter Carreau model viscosity function, written as

$$\eta(\Delta)=(\eta_o-\eta_\infty)\,[1+(\lambda\Pi_\Delta)^2]^{(n-1)2}+\eta_\infty \tag{5}$$

where Π_Δ is the second invariant of the rate of deformation tensor, Δ.

$$\Pi_\Delta^2=2\left(\frac{\partial u}{\partial x}\right)^2+\left(\frac{\partial u}{\partial y}+\frac{\partial v}{\partial x}\right)^2+2\left(\frac{\partial v}{\partial y}\right)^2 \tag{6}$$

Note: When $n=1$, Eq. 5 reduces to the Newtonian fluid model: $\eta(\Delta)=\eta_o$.

Figure 1a illustrates the blade coater geometry. The perimeter of this domain (not the final computational domain, see Figure 2a) is divided into six segments in Figure 1b, for ease in referring to the various regions over which appropriate boundary conditions must be prescribed for modeling purposes. The simplest boundary conditions reflect the assumed no-slip kinematic condition on both the roll and blade surfaces. On the moving roll, segment 1, this no-slip constraint translates into the following boundary conditions on velocity

$$u=U\left(\frac{R+y}{R}\right) \tag{7}$$

$$v=-U\frac{x}{R} \tag{8}$$

while on the stationary blade, segment 4,

$$u=0 \tag{9}$$

$$v=0 \tag{10}$$

At some distance downstream there is a boundary, segment 2, across which the coated film is assumed to move in rigid rotation with the roll (this assumption is verified in Figure 7). Since Cartesian coordinates are chosen, this simple kinematic condition takes the algebraic form

$$u=U\frac{r}{R}\left(\frac{R+y}{R}\right) \tag{11}$$

$$v=-U\frac{rx}{R^2} \tag{12}$$

where

$$r=[(R+y)^2+x^2]^{1/2} \tag{13}$$

Although the velocity profile across the outlet boundary is specified, the flow rate (i.e., coating thickness) is not constrained, because the final *length* of the boundary depends on the *a priori* unknown free surface height.

Along the free surface, segment 3, that separates from the downstream corner of the blade, we impose conditions on the stress and the kinematics. The kinematic condition is simply that there is no mass flux across the free surface, or

$$v\cdot n=0 \tag{14}$$

We also assume that the gas phase exerts no shear stress on the interface and that normal stress at the free surface is balanced by a stress arising from the interfacial tension of the liquid, and the interface curvature. In terms of the Cauchy stress sensor T

$$T=-pI+\tau \tag{15}$$

these conditions take the form

$$nt:T=0 \tag{16}$$

$$nn:T=\sigma\frac{\partial t}{\partial s} \tag{17}$$

In the equations above, n and t are the unit normal and tangent vectors at the free surface, and s is the arc length coordinate (ambient pressure is assumed to be zero).

To complete a model of the coating process, it is necessary to specify boundary conditions for the region upstream of the

blade. Unlike segments 1 through 4, which are easily assigned reasonable boundary conditions, the upstream region, segments 5 and 6, presents a formidable problem. The source of this problem is that boundary conditions along the inlet, segment 6, coupled with those for the upstream free surface position, segment 5, must not constrain the flow rate (i.e., coating thickness). It is not clear how to couple these boundary conditions realistically in a convergent numerical scheme without constraining the flow rate.

Our experimental observation is that fluid entrained from the reservoir by the motion of the roll *floods* the upstream region of the blade. Some fluid passes under the blade and the remainder forms a recirculating region and flows back to the bath. For a *sufficiently flooded* upstream region, it is observed that the coating thickness (i.e., the amount of fluid passing under the blade) is independent of the amount of fluid entrained from the bath and the size of the recirculating region. In light of this experimental observation, and in the absence of a more realistic alternative, we simplify the upstream region by treating it as if it were an infinite bath of fluid; see Figure 2a. We discuss this aspect of the problem as part of the description of the numerical solution procedure.

Numerical Solution Procedure

The governing equations, Eqs. 1–6, are solved by the finite-element method. The theoretical foundation for the method can be found in Zienkiewicz (1977) and Crochet et al. (1984), and a good discussion of the considerations associated with free-surface problems is presented by Kistler and Scriven (1984). Figure 2a shows a typical finite-element mesh ($W = 0.0131$ m, $\omega = 0°$, and $Ho = 0.00127$ m), made up of nine-node isoparametric quadrilateral elements, over which the velocities and pressure are approximated using biquadratic and bilinear basis functions, respectively. We approximate the shape of the downstream free surface with one-dimensional quadratic basis functions and specify that the upstream end is pinned to the downstream corner of the blade, while the opposite end remains tangent to the roll surface. Galerkin's method is used to minimize the "residuals," which results in a system of nonlinear equations, where the nonlinearities arise from the inertial terms,

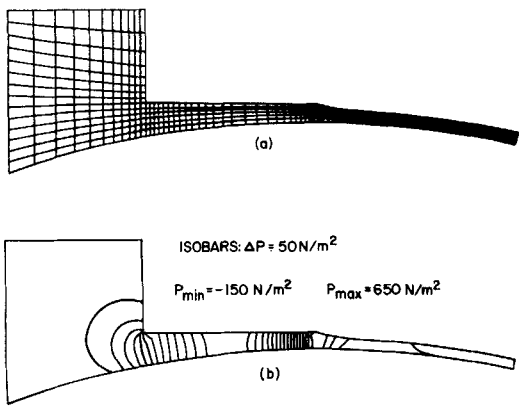

Figure 2. (a) Typical finite-element mesh.
$W = 0.0131$ m; $Ho = 0.00127$ m; $\omega = 0°$

(b) Resulting pressure distribution and free surface shape for a Newtonian liquid.
$\eta_o = 1.0$ kg/m · s

the constitutive Eqs. 4, 5, and 6, and the presence of the free surface. This system of equations is solved for nodal values of the dependent variables (velocities, pressure, and the length of "spines" extending from each free surface node to the roll surface) by full Newton-Raphson iteration. Details of the procedure are given in Sullivan (1986).

It is difficult to apply boundary conditions along the upstream region, segments 5 and 6 in Figure 1b, with confidence, so we have chosen to utilize a simplifying infinite bath assumption. In order to model the upstream region as an infinite bath of fluid, one must arbitrarily locate a domain boundary within the infinite bath and specify appropriate boundary conditions. We treat the uncertainty associated with this boundary in the following manner. We assume that when the upstream domain boundary is "far" from the entrance region formed by the blade and the roll, the traction ($\boldsymbol{n} \cdot \boldsymbol{T}$) along that boundary will be negligible relative to stresses that develop in the vicinity of the blade. With this assumption, a no-traction boundary condition is applied along the upstream region of the mesh.

$$\boldsymbol{n} \cdot \boldsymbol{T} = 0 \tag{18}$$

In order to confirm that the upstream boundary of the mesh is "far" enough from the entrance region and to justify applying the no-traction boundary condition, we solve the set of equations with different boundary locations and demonstrate that the final results (coating thickness in particular) become independent of boundary location.

In addition to the roll radius ($R = 0.07$ m), coater geometry is defined by three parameters shown in Figure 1a: blade width ($W = 0.0131$ and 0.0017 m), blade angle ($\omega = 0°$ and 10°), and blade height ($Ho = 0.00127$, 0.000762, and 0.000254 m). These parameters, as well as the roll speed ($\Omega = 0.58$ s^{-1}) and fluid properties, Table 3, were selected to provide a direct comparison with experiments. This direct comparison facilitated an objective evaluation of the upstream boundary conditions. For a given blade-over-roll coater geometry, the solution procedure is summarized as follows:

1. Choose a reasonable upstream boundary location and generate a mesh for the particular domain, including a reasonable guess at the free surface location.
2. Starting with an initial velocity field and pressure distribution of zero, solve the linearized "stick-slip" problem in order to generate an initial velocity field and pressure distribution for the nonlinear problem. The stick-slip problem is linearized by neglecting inertia, assuming Newtonian behavior, and fixing the free surface location (allowing tangential slip along that surface).
3. Starting with the results of the stick-slip problem, solve the nonlinear (inertia and free surface included) problem for a Newtonian fluid (i.e., $n = 1$ in Eq. 5).
4. Starting with the Newtonian results, solve the nonlinear problem again, with the Carreau model constitutive equation, having parameters appropriate for the particular non-Newtonian liquid of interest [i.e., 1.25% carboxylmethylcellulose (CMC); see Table 1 and Figure 3].
5. Choose a more refined mesh and repeat steps 2 through 4 until satisfied that the solution is independent of mesh size.
6. Repeat steps 1 through 5 for different upstream boundary locations until satisfied that the solution is independent of boundary placement.

Table 1. Physical Properties of Fluids Used in Finite-Element Simulations

Newtonian Model*	
ρ	1,300 kg/m^3
σ	0.069 N/m
η_o	1.0 kg/m · s
Carreau Model**	
ρ	1,000 kg/m^3
σ	0.076 N/m
η_o	1.7 kg/m · s
η_∞	0.01 kg/m · s
Λ	0.22 s
n	0.52

*50/49/1 Karo syrup/glycerine/water solution
**Carreau model parameters chosen to curve-fit viscosity vs. shear rate data for 1.25% CMC, Figure 3

Table 2. Physical Properties of Experimental Newtonian Test Liquids

Fluid	η_o kg/m · s	σ N/m	ρ kg/m^3
Glycerol	0.5–1	0.063	1,260
Karo syrup	3.8	0.075	1,380
Karo syrup/glycerol/water 50/49/1 by vol.	1.0	0.069	1,310

Fluids Studied

Three Newtonian fluids were prepared and studied, glycerol, corn syrup (Karo), and an aqueous mixture of these two base fluids. Table 2 gives the relevant properties, as measured by standard methods. A detailed discussion of fluid property measurements and considerations that led to selection of these three fluids are given in Sullivan (1986).

Four viscoelastic fluids were prepared; a partial list of fluid properties is given in Table 3. Three fluids used a 1.25 wt. % aqueous solution of carboxymethylcellulose (CMC; Hercules 7H) in deionized water as a base fluid. Small amounts of high molecular weight polyacrylamide (Dow Separan AP-273, MW $\approx 2\times10^6$) were added to two of these fluids to give different degrees of elasticity without a significant change in shear viscosity. The fourth fluid was an aqueous solution containing 96.3% wt. % of corn syrup to which 500 ppm polyacrylamide had been added. This produced a "Boger fluid" (Boger, 1976), a fluid with a nearly Newtonian shear viscosity, but with a large normal stress difference.

Rheological properties of the viscoelastic fluids were measured in a Rheometrics fluids rheometer using both Couette and cone-and-plate geometries. The steady shear viscosity,

Table 3. Physical Properties of Experimental Non-Newtonian Test Liquids

Fluid	n	σ N/m	ρ kg/m^3
1.25% CMC in DI Water	0.52	0.076	1,000
1.25% CMC and 0.005% Sep AP-273	0.52	0.076	1,000
1.25% CMC and 0.020% Sep AP-273	0.52	0.076	1,000
Boger fluid	0.97	0.075	1,350

CMC: carboxymethylcellulose
Sep AP-273: Dow Separan polyacrylamide

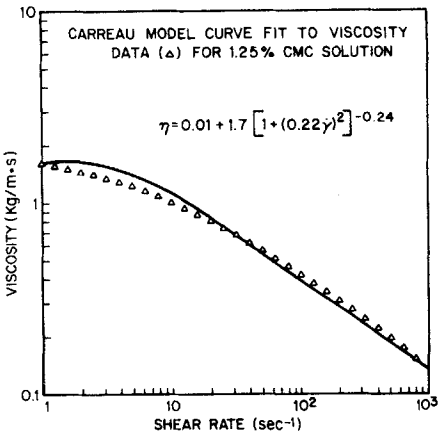

Figure 3. Carreau model curve fit, viscosity vs. shear rate data.

$\eta(\dot{\gamma})$, and the primary normal stress difference (in steady shear), $N1(\dot{\gamma})$, are shown in Figure 4. As a means of ranking these fluids according to their relative degrees of elasticity, we use the steady recoverable shear, S_R, defined by

$$S_R = \frac{N1}{2\eta\dot{\gamma}} \tag{19}$$

Figure 5 shows these data. When possible, rheological data were obtained in the shear rate range of 1 to 1,000 s^{-1}, which coincides with the range of nominal shear rates U/Ho present in the coating experiments.

Film Thickness Measurement

A laboratory scale blade-over-roll coater, Figure 6, was designed specifically for the purpose of generating coating thickness data for a variety of test liquids over a wide range of coater geometries. A stainless steel roll, 0.14 m dia. and 0.127 m long, is driven by a constant-speed motor. The roll is supported by sealed bearings mounted in the walls of an acrylic box that serves as a reservoir for the test fluids. Fluid is entrained from the reservoir by the motion of the roll and wiped by a rigid alu-

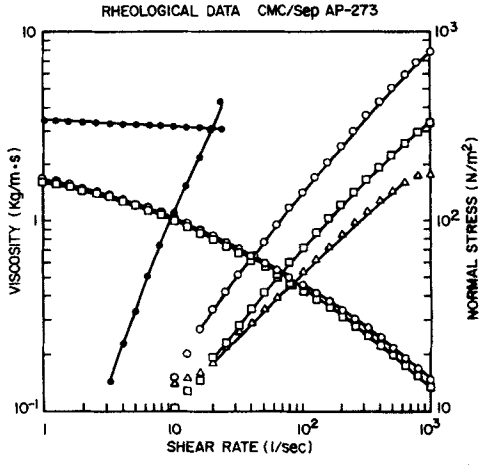

Figure 4. Viscosity and normal stress as a function of shear rate for CMC solutions and Boger fluid.

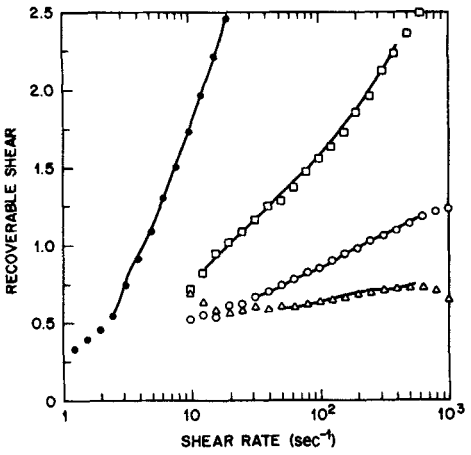

Figure 5. Recoverable shear, Eq. 19, as a function of shear rate.

Non-Newtonian test fluids:
△ 1.25% CMC
○ 1.25% CMC and 0.005% Sep AP-273
□ 1.25% CMC and 0.020% Sep AP-273
● Boger fluid

minum blade. Interchangeable blades can be mounted on a micrometer-driven blade holder and accurately positioned relative to the roll surface. Coating thickness is measured far downstream of the blade by observing contact with the fluid surface by a micrometer-driven needle. Contact of the needle with the surface is observed through a microscope.

A discussion of the details of the experimental procedures for fixing the position of the blade relative to the roll and measuring the coating thickness is given in Sullivan (1986) and Sullivan and Middleman (1986). Results are presented in the form of coating thickness h vs. blade height Ho, each plot corresponding to a particular geometry, test fluid, and operating conditions (i.e., roll speed and temperature). It is estimated that blade height and coating thickness are accurate to ± 25 μm.

For results presented here, all blades are positioned with the

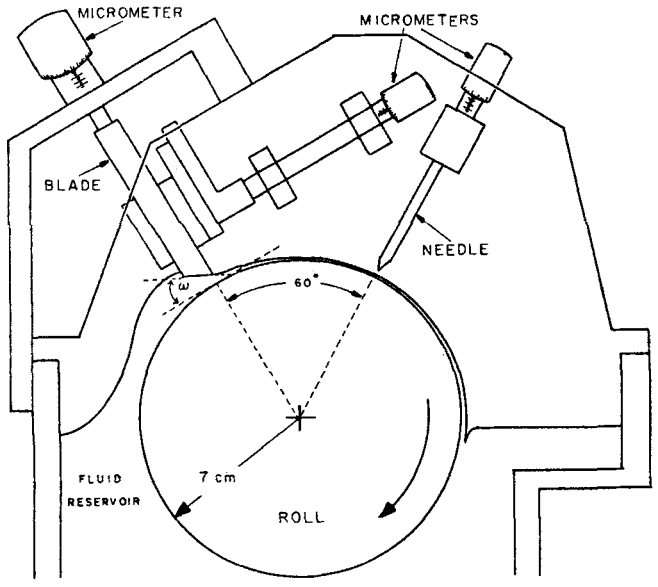

Figure 6. Experimental blade-over-roll coater.

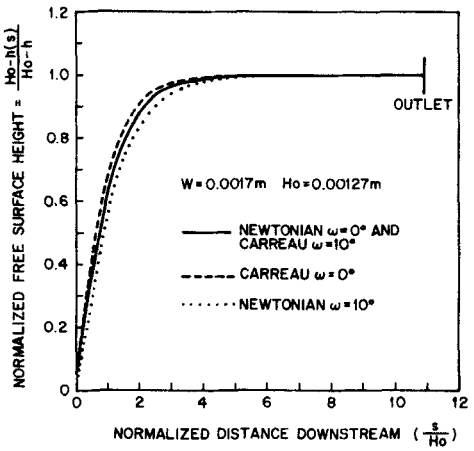

Figure 7. Normalized free surface height as a function of distance downstream of blade.

blade tip (the point of closest approach) located directly above the vertical roll radius (i.e., $x = 0$ in Figure 1a). Blade angles ω of 0° and 10° are reported for two different blade widths, W = 0.0131 and 0.0017 m. We refer to these blades as "large" and "small," respectively. Only a selection of data is presented here; additional results may be found in Sullivan (1986).

Results

Finite-element simulations were carried out for two purely viscous fluids, one Newtonian and one non-Newtonian (shear thinning), in twelve coater geometries. Geometric parameters, fluid properties, and operating conditions (i.e., roll speed) were chosen to provide direct comparison with experiments. Numerical justification for the outlet boundary conditions, Eqs. 11 and 12, and an indication of the rate at which the free surface "relaxes" to the final height can be found in Figure 7.

Consistent with our previous results (Sullivan and Middleman, 1986), data for coating thickness h as a function of blade height Ho for several Newtonian liquids are wholly in agreement with lubrication theory for large blades, Figure 8, but show a larger film thickness, in comparison to the prediction of

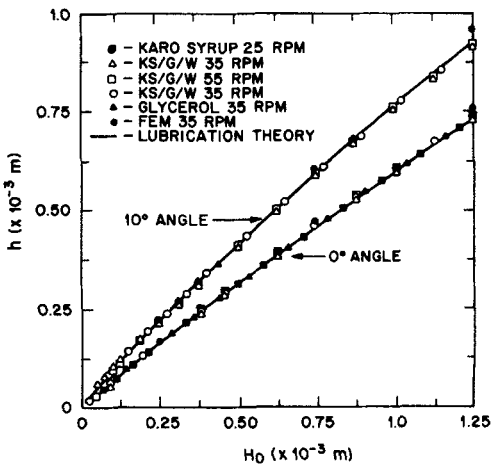

Figure 8. Newtonian fluids: coating thickness as a function of blade height.

Large blade, W = 0.0131 m

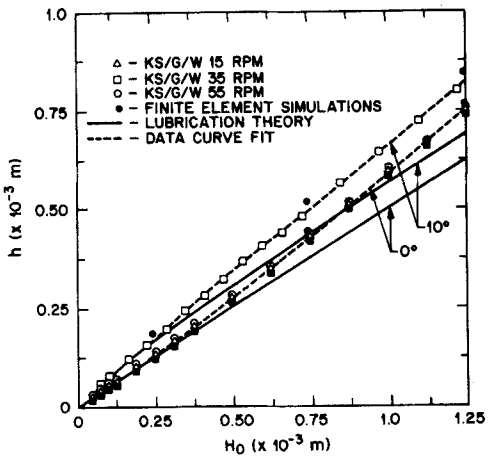

Figure 9. Newtonian fluids: coating thickness as a function of blade height.
Smallest blade, $W = 0.0017$ m

lubrication theory, for small blades, Figure 9. Finite-element simulations, however, agree very well with Newtonian data for both large and small blades.

In addition to solving a simplified set of governing equations, lubrication theory models require that some simplifying assumption be made with regard to inflow and outflow boundary conditions. Boundary conditions at the ends of the blade are not at all obvious and have been the subject of debate for a number of similar converging-diverging flow problems involving free surfaces (Coyne and Elrod, 1970; Birkoff and Hayes, 1963; Savage, 1977; Taylor, 1974). In our previous lubrication analysis (Sullivan and Middleman, 1986), we specified ambient pressure at both ends of the blade. Our reasoning was that the lubrication approximations would be valid only under circumstances when the hydrodynamics under the blade dominate any external influence at the ends of the blade. Also, by choosing these conditions the solution procedure was greatly simplified, with what was hoped to be a minimal effect on the results (Pearson, 1967).

The assumption of our previous analysis, that ambient pressure exists at both ends of the blade, has been found to greatly restrict the range of applicability of the lubrication theory model. Figure 10 provides a comparison between pressure distributions obtained from lubrication theory calculations and those from finite-element simulations (large blade at both 0° and 10° angles). Pressures from the finite-element simulations correspond to nodes midway between the blade and roll surfaces. Typical isobars are shown in Figure 2b to demonstrate the slight variation in pressure across the gap. For these particular (large blade) geometries, results from both lubrication theory and finite-element simulations are in fairly good agreement with regard to coating thickness. However, using finite-element simulations to determine pressure boundary conditions for the lubrication theory model provides even better agreement between both the coating thickness and the pressure distributions. Values for coating thickness agree to within 1.5% when corrected boundary conditions are used in the lubrication analysis, as compared to 5% when they are not. In Figure 10, the pressure is plotted in dimensionless form P^*, where

$$P^* = \frac{pHo}{2\pi R\Omega\eta} \tag{20}$$

In Equation 20, the viscosity η corresponds to η_o for Newtonian results and to the steady shear viscosity at a nominal shear rate ($\dot{\gamma}_N = 2\pi R\Omega/Ho$) of 200 s^{-1} for non-Newtonian results [$\eta(200\ s^{-1}) = 0.27$ kg/m · s].

An even more dramatic improvement is obtained for small blade geometries, as shown in Figure 11. Here, ambient pressure boundary conditions are obviously inadequate, because the pressure distributions predicted by lubrication theory deviate significantly from the finite-element simulations. This deviation can be almost completely eliminated by specifying pressure boun-

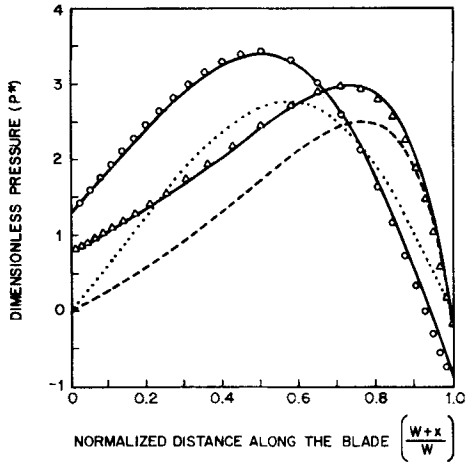

Figure 10. Newtonian fluid: pressure distribution under large blade.
$W = 0.131$ m; $Ho = 0.00127$ m
Δ $\omega = 0°$, O $\omega = 10°$, finite-element simulations
--- $\omega = 0°$, · · · $\omega = 10°$, lubrication theory with ambient pressure boundary conditions
— Lubrication theory using finite-element results to specify pressure boundary conditions

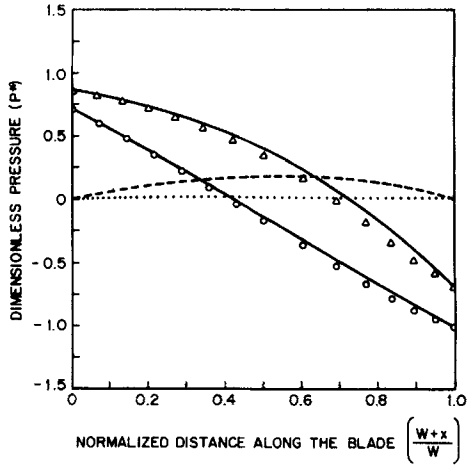

Figure 11. Newtonian fluid: pressure distribution under small blade.
$W = 0.0017$ m; $Ho = 0.00127$ m
Δ $\omega = 0°$, O $\omega = 10°$, finite-element simulations
--- $\omega = 0°$, · · · $\omega = 10°$, lubrication theory with ambient pressure boundary conditions
— Lubrication theory using finite-element results to specify pressure boundary conditions

dary conditions for the lubrication theory model using the finite-element results. Both the pressure distributions *and* coating thickness predictions then show very good agreement: coating thickness agrees to within 1%, as compared to the 20% discrepancy obtained using ambient pressure boundary conditions. Failure of the lubrication theory model for small blades under the experimental conditions prevailing in this study, therefore, appears to be caused by the lack of appropriate inflow and outflow boundary conditions. Unfortunately, these results do not indicate how one might specify appropriate boundary conditions for the lubrication theory, because the values provided by the finite element simulations are *a priori* unknown.

For the 1.25% CMC solution, we find that the coating thickness data agree quite well with non-Newtonian (Carreau) finite-element solutions for both large and small blades, Figure 12. This is a significant improvement over simple non-Newtonian (power law) lubrication theory, which underestimates the coating thickness (Sullivan and Middleman, 1986). As in the Newtonian case, simple ambient pressure boundary conditions were used in the non-Newtonian lubrication theory model and, not surprisingly, the model underestimates coating thickness. However, a direct comparison with finite-element results has not been made because the finite-element simulations utilize the four-parameter Carreau model, while the non-Newtonian lubrication theory relied on a simple power law model.

Numerical experiments were conducted to estimate the influence of inertial and surface tension forces on coating thickness in the parameter range corresponding to our experiments. An appropriate Reynolds number Re and capillary number Ca can be defined for the coating process by

$$Re = \frac{\rho 2\pi R\Omega Ho^2}{\eta W} \tag{21}$$

$$Ca = \frac{2\pi R\Omega\eta}{\sigma} \tag{22}$$

In these equations, values for η are identical to those discussed for Eq. 20. Under the experimental conditions considered in this study, $Re_{max} = 0.9$ and inertial effects were found to be negligible in numerical experiments (less than 1% variation in λ). Surface tension effects were also negligible, even though Ca was not large ($Ca < 4$). This is due to the minimal amount of curvature at the free surface, which can be observed in Figure 2. The numerical results are summarized in Table 4, accompanied by experimentally measured values of coating thickness.

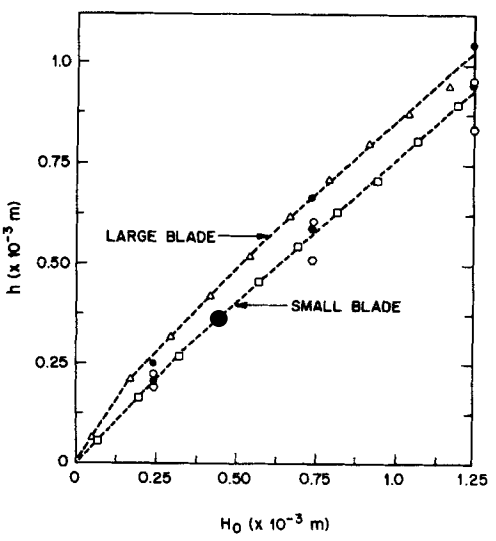

Figure 12. Coating thickness as a function of blade height for blades at 10° angle.

Table 4. Results from Finite-Element Simulations for Dimensionless Coating Thickness*

Blade Angle	Newtonian $\eta_o = 1.0$ kg/m · s $Re = 0.041$ $Ca = 3.7$	Carreau $\eta(200\ s^{-1}) = 0.27$ kg/m · s $Re = 0.12$ $Ca = 0.91$
	Large Blade, $W = 0.0131$ m	
0°	$\lambda_{exp} = 0.60$ $\lambda_{fem} = 0.617(0.617)[0.616]$	$\lambda_{exp} = 0.65$ $\lambda_{fem} = 0.660(0.659)[0.661]$
10°	$\lambda_{exp} = 0.74$ $\lambda_{fem} = 0.768(0.768)[0.767]$	$\lambda_{exp} = 0.82$ $\lambda_{fem} = 0.846(0.844)[0.849]$
	Small Blade, $W = 0.0017$ m	
0°	$\lambda_{exp} = 0.60$ $\lambda_{fem} = 0.610(0.609)[0.608]$	$\lambda_{exp} = 0.70$ $\lambda_{fem} = 0.689(0.682)[0.687]$
10°	$\lambda_{exp} = 0.66$ $\lambda_{fem} = 0.679(0.679)[0.678]$	$\lambda_{exp} = 0.76$ $\lambda_{fem} = 0.768(0.763)[0.769]$

*$\lambda = h/Ho$; roll speed 0.26 m/s; blade height 0.00127 m
λ_{exp} = λ from experiments
λ_{fem} = λ from finite-element simulations
( ) = result without surface tension included (i.e., $Ca \to \infty$)
[ ] = result without inertial terms included (i.e., $Re \to 0$)

Although the finite-element simulations do not include elastic effects, it is possible to estimate the impact elasticity has on the coating process through a series of controlled experiments using liquids with very similar shear viscosities, Figure 4, but significantly different degrees of elasticity as measured by their steady normal stress behavior. Since the Carreau model finite-element simulations agree well with experimental data for the 1.25% CMC solution, that solution appears to behave as a purely viscous liquid. No phenomena that can be attributed to the viscoelastic character of the liquid are observed. Hence, these data provide a baseline against which data for more elastic liquids can be compared. From results presented in Figure 13, increasing elasticity can now be seen to reduce the coating thickness. In fact, the coating thickness for a shear-thinning fluid can be reduced below that of a Newtonian liquid if the fluid is sufficiently *elastic*. Data for the highly elastic Boger fluid, which on a purely viscous basis would appear Newtonian, are also presented in Figure 13. Again it is observed that the coating thickness is reduced well below the level expected on the basis of the purely viscous behavior of this liquid.

The Boger fluid data show an even more remarkable result. For Newtonian liquids, the coating thickness vs. blade height data depend strongly on blade angle and blade width. Figure 14 shows that for the highly elastic Boger fluid, these data are essentially invariant with geometry in the range studied. There is something unusual about the kinematic behavior of a highly elastic fluid, in the flow field studied here.

Discussion

It is clear that fluid rheology has a significant impact on coating thickness in a blade coater. Relative to Newtonian liquids, either an increase or decrease in coating thickness can be

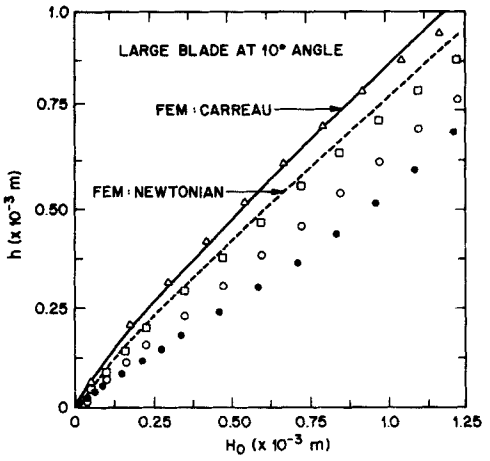

Figure 13. Coating thickness as a function of blade height, large blade, 10° angle.

△ 1.25% CMC
□ 1.25% CMC and 0.005% Sep AP-273
○ 1.25% CMC and 0.020% Sep AP-273
● Boger fluid

observed when coating viscoelastic liquids, and these trends appear to correlate with the shear thinning and elastic behavior of the fluids (as measured in steady shear flow). In agreement with our experiments and a number of previous theoretical studies (Middleman, 1977; Guzy and Higgins, 1982), finite-element simulations predict that coating thickness is greater for purely viscous shear-thinning liquids than it is for constant viscosity (i.e., Newtonian) liquids. However, these simulations do not include elasticity, which is observed experimentally to cause a reduction in the coating thickness.

Consistent with this result is an observation made by Doremus and Piau (1981, 1983) regarding flow in a similar geometry (flow between a small stationary cylinder and a large rotating drum), for which they report: "very much less fluid is carried through the gap for viscoelastic solutions, compared with Newtonian liquids under similar experimental conditions." This observation contradicts the results of theoretical models based on purely viscous behavior, which suggest that *more* fluid would pass through the gap (i.e., the coating thickness is higher) with a shear-thinning liquid.

The precise mechanism by which elasticity causes the coating thickness to decrease is subject to speculation. The blade coating process is predominantly a shear flow and it is doubtful that extension rates (or extensional viscosities) are large enough to generate the dramatic decrease in coating thickness observed. The significant effect elasticity has on transient fluid properties may provide the most likely explanation. Although blade coating is a steady state process, fluid particles undergo a rapid Lagrangian acceleration under the blade and, therefore, experience a rapidly changing deformation history. One estimate of the time scale involved is the residence time of a fluid particle under the blade, or

$$t_{res} = \frac{W}{2U} \tag{23}$$

For the smallest blade ($W = 0.0017$ m) at a roll speed of 0.26 m/s, t_{res} is on the order 0.007 s. We can use the recoverable shear to estimate a Maxwell relaxation time for the test fluids by

$$t_{relax} = \frac{S_R}{\dot{\gamma}} \tag{24}$$

Figure 4 indicates that at a nominal shear rate U/Ho of 200 s^{-1}, approximate relaxation times for the three CMC solutions are 0.003, 0.005, and 0.010 s. We see that the relaxation times of these fluids are of the same order of magnitude as transients in the flow field, and we suspect that it is the influence of elasticity on the transient response of these fluids that is responsible for the observed decrease in coating thickness with increasing elasticity.

In contrast to Newtonian results, the coating thickness for viscoelastic liquids showed a slight dependence on roll speed (Sullivan, 1986). Coating thickness was observed to decrease slightly with an increase in roll speed.

Doremus and Piau (1983) also observed a speed effect with non-Newtonian liquids, using a flow visualization technique. In contrast to Newtonian liquids, which were unaffected by drum speed, the stagnation point (i.e., where the stagnation streamline intersects the solid boundary) for non-Newtonian liquids moved closer to the gap with increasing drum speed. This suggests that viscoelastic liquids experience a more restricted area of entrance (defined by the stagnation streamline) with increasing speed, which is consistent with our observation that coating thickness decreases. Metzner (1971) also observed a narrowing entrance region for viscoelastic liquids when studying flow through abrupt contractions.

Narrowing of the entrance region by a displaced stagnation streamline could explain the result that the coating thickness of the highly elastic Boger fluid appears to be independent of the upstream blade geometry, Figure 14. One possible explanation is that elasticity causes the stagnation point to move toward the point of minimum separation between the blade and the roll, such that the stagnation streamline and not the upstream blade geometry defines the entrance region experienced by the fluid. Assuming that the stagnation streamline is unaffected by the upstream blade geometry (e.g., remains pinned at the point of minimum separation between the roll and blade), then the coating thickness would appear to be independent of upstream blade geometry. For example, consider the streamlines obtained from

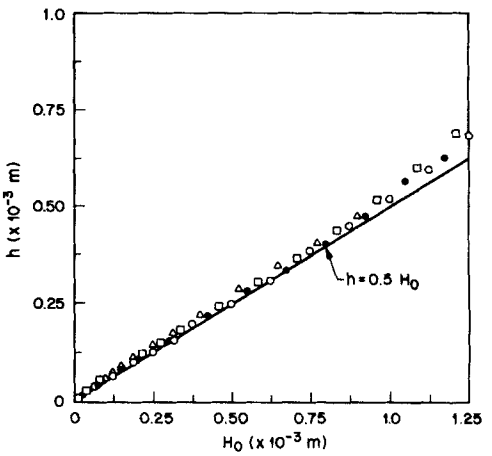

Figure 14. Negligible effect of geometry on coating thickness for highly elastic Boger fluid.

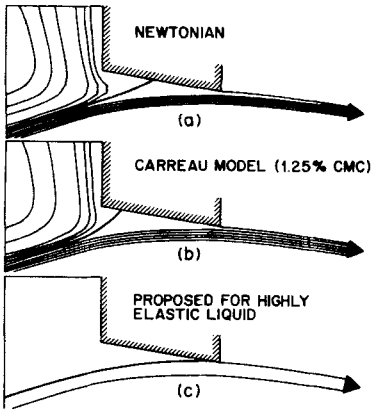

Figure 15. Finite-element simulations of streamlines.
(a) (b) $W = 0.0131$ m; $\omega = 10°$; Ho $= 0.00127$ m ($\Delta\psi = 0.2$) (c) Stagnation streamline, $\psi = 1.0$

the finite-element simulations for a Newtonian and a shear-thinning fluid shown in Figures 15a and 15b, respectively. Here, the stream function ψ has been normalized to take on the value zero at the roll and unity along the free surface. Observed differences in flow rate (i.e., coating thickness) are reflected by the location at which the stagnation streamline (i.e., $\psi = 1.0$) intersects the blade surface. The intersection point is closer to the forward blade tip for the lower flow rate of the Newtonian liquid than it is for the shear-thinning liquid. We propose that the Boger fluid, which exhibits an even lower flow rate experimentally, must have a stagnation streamline that is displaced even closer to the blade tip. As this stagnation streamline approaches the blade tip, one would expect the influence of the upstream blade geometry to diminish. If the stagnation streamline were as postulated in Figure 15c, then the fluid would "believe" it was being coated by a long parallel (and nearly plane, since $Ho \ll R$) blade, for which the coating thickness would be $h = 0.5\ Ho$ under all conditions. This is in fact essentially what is observed with the data in Figure 14.

In our experiments, coater geometry was fixed and independent of the magnitude of hydrodynamic pressure. In most industrial coating operations the pressure distribution determines the loading on the blade, which in turn sets the gap (i.e., blade height). Industrial blade coaters can operate at speeds in excess of 15 m/s (e.g., paper coating) and it would be worthwhile to have some quantitative estimate of the effect of inertia. Unfortunately, it is not a trivial task to extend the finite-element simulations to high Re with confidence. Mesh refinement requires careful consideration and the computational domain upstream of the blade must be extended beyond any strong recirculation patterns in order to allow for the use of the no-traction boundary condition. Recirculation regions are of great interest, since trapped fluid (e.g., dispersions) can set up with time and lead to coating defects. A considerable amount of computing resources would be required to investigate higher Re conditions. For this reason we have limited our efforts to simulations corresponding to experimental conditions for which we have data and leave the higher Re simulations for future studies.

Conclusions

Finite-element simulations for purely viscous liquids are in very good agreement with experimental measurements of coating thickness for Newtonian and relatively inelastic non-Newtonian (i.e., an aqueous 1.25% CMC solution) liquids. Pressure distributions obtained from finite-element simulations reveal that the use of simple ambient pressure boundary conditions in the lubrication theory significantly limits the applicability of such models and results in an underestimate of the coating thickness.

Fluid rheology is found to have a significant impact on coating thickness in a blade coater. Purely viscous shear-thinning behavior results in an increased coating thickness relative to Newtonian results. Viscoelastic liquids, characterized by their viscosity (shear thinning) and normal stress (elastic) behavior in steady shear flow, exhibit either an increase or decrease in coating thickness relative to Newtonian liquids, depending on the relative contribution of shear-thinning and elastic effects. Increasing elasticity leads to a decrease in coating thickness, as demonstrated by experimental measurements of coating thickness for a series of viscoelastic liquids having almost identical viscosity behavior, but different elasticity. Of particular interest is the observation that the coating thickness for a highly elastic Boger fluid appears to be independent of blade geometry, in contrast to Newtonian results, which show a significant dependence on blade angle and width.

Acknowledgment

Grateful acknowledgement is made by T. Sullivan and S. Middleman for the support of the Center for Magnetic Recording Research of the University of California, San Diego. The work of Roland Keunings was supported by the Director, Office of Energy Research, Office of Basic Energy Sciences, Material Science Division of the U.S. Department of Energy under Contract No. DE-AC03-76SF00098.

Notation

Ca = capillary number, Eq. 22
h = coating thickness, m
Ho = blade height at $x = 0$, m
I = identity tensor
n = power law index
$\boldsymbol{n}$ = unit normal vector
$N1$ = normal stress difference, N/m^2
p = pressure, N/m^2
P^* = dimensionless pressure, Eq. 20
r = radial coordinate with respect to roll, m
R = roll radius, m
Re = Reynolds number, Eq. 21
s = arc length, m
S_R = recoverable shear
T = Cauchy stress tensor, N/m^2
t = unit tangent vector
t_{res} = residence time, s
t_{relax} = relaxation time, s
u = x component of velocity, m/s
U = linear roll speed, m/s
$\boldsymbol{v}$ = velocity vector, m/s
v = y component of velocity, m/s
W = blade width, m
x = primary flow direction, m
y = transverse flow direction, m

Greek letters

$\dot{\gamma}$ = shear rate, s^{-1}
$\dot{\gamma}_N$ = nominal shear rate
Δ = rate of deformation tensor, s^{-1}
η = non-Newtonian viscosity, kg/m · s
η_o = zero shear or Newtonian viscosity, kg/m · s
η_∞ = infinite shear viscosity, kg/m · s
Λ = Carreau model parameter

λ = dimensionless coating thickness, h/Ho
ρ = density, kg/m^3
σ = surface tension, N/m
τ = extra stress tensor, N/m^2
τ_{ij} = component of the extra stress tensor, N/m^2
ψ = normalized stream function
ω = blade angle, degrees
Ω = roll speed, s^{-1}
I = identity tensor
Π_Δ = second invariant of the rate of deformation tensor, s^{-2}

Literature Cited

Boger, D. V., "A Highly Elastic Constant-Viscosity Fluid," *J. Non-Newt. Fluid Mech.*, **3,** 87 (1976).

Birkoff, G., and D. F. Hayes, "Free Boundaries in Partial Lubrication," *J. Math. Phys.*, **42,** 129 (1963).

Cameron, A., *Principles of Lubrication,* Longmans, London (1966).

Coyne, J. C., and H. G. Elrod, Jr., "Conditions for the Rupture of a Lubricating Film. II: New Boundary Conditions for Reynold's Equations," *ASME Paper No. 70-Lub-3* (1970).

Crochet, M. J., A. R. Davies, and K. Walters, *Numerical Simulation of Non-Newtonian Flow,* Elsevier, Amsterdam (1984).

Doremus, P., and J-M. Piau, "Viscoelastic Elongational Lubrication," *J. Non-Newt. Fluid Mech.*, **9,** 389 (1981).

———, "Experimental Study of Viscoelastic Effects in a Cylinder-Plane Lubricated Contact," *J. Non-Newt. Fluid Mech.*, **13,** 79 (1983).

Guzy, C. J., and B. G. Higgins, "Viscous Pressure Drop Across the Nip of a Blade Coater and Its Effect on the Final Coated Film Thickness," *Proc. TAPPI Coating Conf.* (1982).

Kistler, S. F., and L. E. Scriven, "Coating Flows," *Computational Analysis of Polymer Processing,* J. Pearson, S. M. Richardson, eds., Applied Science, New York, ch. 8 (1984).

Metzner, A. B., "Extensional Primary Field Approximations for Viscoelastic Media," *Rheol. Acta,* **10,** 434 (1971).

Middleman, S., *Fundamentals of Polymer Processing,* McGraw-Hill, New York (1977).

Pearson, J. R. A., "The Lubrication Approximation Applied to Non-Newtonian Flow Problems: A Perturbation Approach," *Nonlinear Partial Differential Equations,* W. F. Ames, ed., Academic Press, New York (1967).

Savage, M. D., "Cavitation in Lubrication. I: On Boundary Conditions and Cavity-Fluid Interfaces," *J. Fluid. Mech.*, **80,** 743 (1977).

Sullivan, T., "An Experimental and Computational Investigation of Rheological Effects in Blade Coating," Ph.D. Thesis, Univ. California, San Diego (1986).

Sullivan, T., and S. Middleman, "Film Thickness in Blade Coating of Viscous and Viscoelastic Liquids," *J. Non-Newt. Fluid Mech.*, **21,** 13 (1986).

Taylor, C. M., "Film Rupture for a Lubricated Cylinder Lightly Loaded Against a Plane," *J. Mech. Eng. Sci.*, **16,** 225 (1974).

Zienkiewicz, O. C. *The Finite-Element Method,* McGraw-Hill, London (1977).

Manuscript received Oct. 10, 1986, and revision received June 26, 1987.